MASSACHUSETTS INSTITUTE OF TECHNOLOGY
CENTER FOR SPACE RESEARCH
CAMBRIDGE, MASSACHUSETTS 02139-4307

Administrative Offices 37-287

April 17, 1992

Ms. M.E. Robinson, Grant Administrator
Mail Code AP32J
NASA, George C. Marshall Space Flight Center
Marshall Space Flight Center, Alabama 35812

RE: Final Technical Report for NAG8-762 "GINGA Studies of X-Ray Scattering and Fluorescence in Massive X-Ray Binaries", PI: Professor Saul Rappaport

Dear Ms. Robinson:

The Center for Space Research at the Massachusetts Institute of Technology hereby submits one copy of the progress report for the above referenced grant.

If you have any further questions of an administrative nature please call me at (617) 253-6103. Questions of a technical nature should be directed to Professor Rappaport (617) 253-7551. Thank you for your help.

Sincerely,

Paula M. Suvanto

Paula M. Suvanto, Administrative Officer

Enclosures

XC: Ms. Donna Havrisik, Mail Code EM25, NASA Marshall (2)
T. Marshall, NASA Scientific and Technical Information Facility,
Accessioning Department
800 Elkridge Landing Road, Linthicum Heights, MD 21090 (2)
J Binsack, TL
P. Greer, TL
S. Rappaport
M. Morris, ONR, TL
file

MIT 74618

617-253-6103 Fax: 617-253-0861 pms@space.mit.edu

PENNSTATE

1855

Department of Astronomy & Astrophysics

(814) 865-0418
FAX: (814) 863-3399

The Pennsylvania State University
525 Davey Laboratory
University Park, PA 16802

26 March 1992

Dr. Robert Petre
Goddard Technical Officer
Code 666
Goddard Space Flight Center
Greenbelt, MD 20771

Dear Bob:

The following report for contract NAG 5 1708 is for the period 15 July 1991 to 15 January 1992.

We have received the two observation tapes that were approved for this proposal. The data have been reduced in a preliminary form, indicating that the observations were successful in achieving the objectives of the proposed research. A seminar was presented at Carnegie Mellon University in December of 1991 and a poster paper was presented at the Atlanta AAS meeting in January on the preliminary results. A paper is in preparation for the Astrophysical Journal which will provide the detailed results, analysis and conclusions of this research project. One professor and one graduate student are working part time on this project.

Sincerely,

Gordon Garmire
Principal Investigator

cc: NSTIF

DEPARTMENT OF PHYSICS
MASSACHUSETTS INSTITUTE OF TECHNOLOGY
CAMBRIDGE, MASSACHUSETTS 02139
37-551

April 7, 1992

IN-13-CR
84318
P-33

Ms. Terri Marshall
NASA Center for Aerospace Information
Acquisitions Department
800 Elkridge Landing Road
Linthicum Heights, MD 21090

Final Technical Report
for NASA Grant NAG8-762

Dear Ms. Marshall:

During the period December 1988 through December 1991 we were supported in part by NASA grant NAG8-762 to conduct Ginga X-ray observations of massive X-ray binary systems. The principal research activities centered about observations of SMC X-1 and LMC X-4 that were made during July and August 1989. Both the principal investigator and the co-investigator were present at the Institute for Space and Astronautical Science in Japan for the observations. The study of these sources was directed toward a determination of the orbital period changes in these massive X-ray binaries. At least two publications will results from these studies: "LMC X-4 - Ginga Observations and Search for Orbital Decay" by A. Levine, S. Rappaport, A. Putney, R. Corbet, and F. Nagase (*Ap. J.*, 1991, **381**, 101) and "Discovery of the Decay of the Orbit of SMC X-1" by A. Levine, S. Rappaport, J. Deeter, P. Boynton, and F. Nagase (*Ap. J.*, 1992, in preparation).

A third massive X-ray binary system was also investigated under this contract. In this case, one of our graduate students (Wayne Lewis) utilized existing Ginga data to study X-ray scattering and fluorescence in the wind of the massive companion to 4U0900-40. Mr. Lewis spent two extended stays of 9 months and 4 months, respectively, at ISAS working on the data analysis. This was followed by the development of an extensive Monte Carlo scattering code to simulate and interpret the observations. This research led directly to a Ph.D. thesis for Mr. Lewis as well as the publication: "X-Ray Scattering and Fluorescence in the Wind of a Massive X-Ray Binary", by W. Lewis, S. Rappaport, A. Levine, and F. Nagase (*Ap. J.*, 1991, **389**, April 20 issue). Portions of this latter paper were written when the PI visited ISAS in the Spring of 1991.

In addition to the above studies, the grant NAG8-762 helped to support several other theoretical studies related to X-ray binaries. These include: "Evolution of Compact Binary Systems With X-Ray Heating" by A. Harpaz and S. Rappaport (*Ap. J.* , 1991, **383**, 739), and "Production of Recycled Pulsars in Globular Clusters via Two-Body Tidal Capture" by R. DiStefano and S. Rappaport (*Ap. J.*, in press).

During the course of this work, one Ph.D. student received partial support and completed his thesis entirely on the research sponsored by this grant. A total of five undergraduates (Bockrath, Cohen, Katalinic, Putney, and Sujono) also derived some support from this grant while working on the research described above as part of the M.I.T. Undergraduate Research Opportunities Program.

Sincerely,

Saul Rappaport

Saul Rappaport
Professor of Physics

DRAFT

Submitted to the Editor of *The Astrophysical Journal* on April 15, 1992

DISCOVERY OF ORBITAL DECAY IN SMC X-1[1]

A. Levine[2], S. Rappaport[2], P. Boynton[3], J. Deeter[3,4], and F. Nagase[4]

CSR-HEA-92-08

[1] This work was supported in part by the National Aeronautics and Space Administration under grants NAG8-762 and NAGW-1545.

[2] Department of Physics and Center for Space Research, Massachusetts Institute of Technology, Cambridge, MA 02139

[3] Department of Astronomy, University of Washington, Seattle, WA

[4] Institute of Space and Astronautical Science, ISAS, Japan

Abstract

We report on the results of three observations of the binary X-ray pulsar SMC X-1 with the Ginga satellite. Timing analyses of the 0.71-s X-ray pulsations yield Doppler delay curves which, in turn, provide the most accurate determination of the SMC X-1 orbital parameters available to date. The orbital phase of the 3.9-day orbit is determined in 1987 May, 1988 August, and 1989 August with accuracies of 11 s, 1 s, and 3.5 s, respectively. These phases are combined with two previous determinations of the orbital phase to yield the rate of change in the orbital period: $\dot{P}_{orb}/P_{orb} = (-3.34 \pm 0.023) \times 10^{-6}$ yr^{-1}. An interpretation of this measurement and the known decay rate for the orbit of Cen X-3 is made in the context of tidal evolution. Finally, a discussion is presented of the relation among the stellar evolution, orbital decay, and neutron-star spinup time scales for the SMC X-1 system.

1. Introduction

Our observations of SMC X-1 were motivated by the similarity of this binary X-ray system with the Cen X-3 system, which led us to speculate that the orbital period of the former system may be changing relatively rapidly as is the case for Cen X-3 ($\dot{P}_{orb}/P_{orb} = -1.8 \times 10^{-6}$ yr^{-1}: Kelley *et al.* 1983b). The time scale for orbital decay of 5×10^5 yr in Cen X-3 is quite short by astronomical standards. Studies of such rapid changes in orbital period are important to understand (i) the underlying cause, e.g., tidal torques related to the Darwin effect (Darwin 1879), and (ii) the lifetime of massive X-ray binaries as the Roche lobe moves through the stellar atmosphere (only ~2000 years in the case of Cen X-3). In particular, we are interested to determine if such rapid changes in orbital period are universal among massive X-ray binaries.

SMC X-1 is one of only three detected extragalactic binary X-ray pulsars (along with LMC X-4 and A0538-66; Primini, Rappaport, and Joss 1977, Bonnet-Bidaud and van der Klis 1981, and references therein). The optical counterpart has been identified with a B0 I supergiant (Sk 160; Webster *et al.* 1972, Liller 1973). X-ray eclipses which occur every 3.89 days were discovered with the Uhuru satellite by Schreier *et al.* (1972). SMC X-1 exhibits low-intensity states in addition to high-intensity states (e.g., Seward and Mitchell 1981, Bonnet-Bidaud and van der Klis 1981); Gruber and Rothschild (1984) suggested, on the basis of HEAO 1 (A4) data, that the source has a 60 day long-term periodicity similar those found in LMC X-4 and Her X-1.

The source brightness, together with the short pulse period (0.71s; Lucke *et al.* 1976) have made SMC X-1 an excellent object for pulse-timing studies. Such studies were initiated with SAS-3 and combined with measurements of the optical velocity curve to yield a projected orbital radius $a_X \sin i = 53.46 \pm 0.05$ ℓt-s, neutron star mass $M_X = 0.8 - 1.8$ $M_\odot$, companion mass $M_C \approx 19$ $M_\odot$, and companion radius $R_C \approx 18$ $R_\odot$ (Primini, Rappaport, and Joss 1977). A list of orbital phase zero measurements for SMC X-1 has been given by Bonnet-Bidaud and van der Klis (1981); this list contains results from observations with Uhuru (in 1971), Copernicus (1975), COS-B (1976), and Ariel 5 (1976), in addition to the SAS-3 measurement. The first three of these orbital phase determinations were based on eclipse data, while the latter two were derived from more accurate pulse-timing analyses. These orbital phase determinations are listed in Table 1. Subsequently, additional observations of SMC X-1 were conducted with HEAO 1 (Gruber and Rothschild 1984), the Einstein Observatory (Darbro *et al.* 1981), and EXOSAT (the EXOSAT log). To our knowledge, however, no additional orbital phase determinations have been reported from these latter observations.

Our Ginga observations of SMC X-1 are described in §II of this paper. Analyses and results pertaining to the timing data and pulse profiles are presented in §III. The results are discussed in §IV.

2. Observations

The observations of SMC X-1 were conducted with the Large Area Counters (LAC) on the Ginga satellite (Makino *et al.* 1987, Turner *et al.* 1989) during three epochs: 3 days in 1987 May, 8.4 days in 1988 August-September, and 4 days during 1989 July-August. Due to earth occultations, crossings of the South Atlantic Anomaly and other high background regions, and performance of telemetry, attitude control, and sky monitoring functions, data on SMC X-1 were obtained with roughly a 30% duty cycle.

The 3-day 1987 May observation was performed during the initial operational test phase of the Ginga satellite, and the data useful for pulse timing were obtained during contact orbits (i.e., the ~5 consecutive orbits per day in which the satellite passes over the Kagoshima, Japan ground station). Much of these data were taken in MPC-3 mode (12 energy channels with 7.8 ms time resolution), but the data obtained during the ~10 minute intervals of actual satellite-ground communication were usually taken in MPC-2 mode (48 energy channels with 62.5 ms time resolution). For the pulse-timing analysis reported here the MPC-3 data were converted to 62.5 ms time resolution by combining time bins, and the energy channels of both modes were combined to yield count rates in the 1-7, 7-14, and 14-23 keV bands. During this observation the X-ray intensity of SMC X-1 was approximately constant at ~90 counts s^{-1} (2-37 keV; ~ 8 μJy at 5 keV).

The 1988 August-September observation was specifically tailored to monitor the X-ray flux of SMC X-1 as continuously as possible, while obtaining data useful for pulse timing. Data were obtained during the intervals 1988 August 24.9 - 28.3 (UT) and 1988 August 31.1 - September 2.7 (UT), but the second interval included an X-ray eclipse. During remote orbits (i.e., the ~10 consecutive orbits each day in which the satellite does not pass over the Kagoshima ground station) the data were obtained exclusively in PC mode (2 energy channels). The energy limits for these channels were chosen to be 1-6 keV (with 31.2 ms time resolution) and 6-24 keV (with 62.5 ms time resolution). [John: which channels do these correspond to?] During contact orbits the observations were similar to those in 1987 May, except that MPC-3 data were generally taken with 62.5 ms time resolution. The X-ray intensity of SMC X-1 outside of eclipse varied between ~25 and ~300 counts s^{-1} (2-37 keV; 2 - 25 μJy at 5 keV). The intensity was particularly low during the time intervals MJD 47398.4 to 47398.7 and 47400.5 to 47401.3 (MJD = JD - 2,400,000.5).

Most of the 1989 data were taken with the MPC 2H and MPC 3M modes which provide

counts in 62.5 ms time bins. Additional data were accumulated in the MPC 2M, MPC 3L, or MPC 3H mode which provided time resolutions of 8 to 500 ms and either 12 or 48 pulse height channels. Only those data having a time resolution of 7.8 or 62.5 ms have been utilized for our pulse-timing analyses. Furthermore, these data were rebinned into 10 energy channels. The equivalent X-ray energies corresponding to these 10 pulse height channels are given in Table 2. The X-ray intensity of SMC X-1 was approximately constant at ~300 counts s^{-1} (2-37 keV; ~ 25 μJy at 5 keV) for most of the observation outside of the eclipse.

3. Analysis and Results

3.1 Temporal Analysis

Pulse timing analyses have been performed with non-background subtracted data which have been selected to exclude the times of the X-ray eclipses, all instances in which the detectors were not operating stably, and all readily apparent noise spikes.

The pulse-timing analysis basically proceeded as follows. The time of observation of each bin of data was converted to coordinated universal time (UTC) and corrected for the relative motion of Ginga and the pulsar according to the known satellite orbit and a provisional orbital ephemeris for SMC X-1. This yields the times of observations that would have been recorded by an instrument moving with an approximately constant velocity relative to the pulsar. The resulting observation times were then used to fold subsets of the data according to a provisional pulsar rotation period and period derivative. Different pulsar orbital and rotational ephemerides were used to reduce the data from each of the three observations. Details of this reduction procedure follow.

The observation times were converted from satellite on-board clock time to UTC. The relation between satellite on-board clock time and UTC was established to an accuracy of 1 ms by comparison of the satellite time with a ground-based standard clock once during each of the five times that the satellite passed over the Kagoshima ground station each day. The stability of the Ginga on-board clock ($\sim 1 \times 10^{-6}$) was sufficient to maintain 1 ms accuracy over the 100-minute interval between consecutive ground contacts (Deeter and Inoue 1990). For remote orbits, however, the use of a mean clock rate between successive clock comparisons (separated by some 17 hours) can result in errors of up to ~20 ms in the conversion of satellite time to UTC. Variations in the Ginga clock rate are largely due to variations in the internal temperature of the satellite (Deeter and Inoue 1990). Using the temperature housekeeping data, we were able to estimate the clock rate and thereby improve the accuracy of time assignments to ~2 ms.

The observation times were corrected for satellite motion relative to the center of the earth using the Ginga orbital ephemeris, and then transformed to the solar system barycenter using the CfA planetary ephemeris (Chandler 1991) or the JPL planetary ephemeris (reference). In

making these corrections we used the coordinates of Sk 160 reported by Clark et al. (1978).

The observation times were also corrected for a provisional pulsar orbit. The results were then used to fold subsets of data from time intervals typically ~2000 s in duration according to a provisional pulse ephemeris. The provisional parameters were sufficiently precise to fold a ~2000 s interval of data with smearing of < 0.1 pulse periods. For the 1987, 88, & 89 observations, a total of 18, 149, and 61 pulse profiles were constructed, respectively.

For each of the three observations a pulse template was constructed by averaging the individual profiles (1987 and 1988 data) or simply by utilizing one of the pulse profiles having particularly good counting statistics (1989 data). Each template was then cross correlated with the individual profiles from that observation to obtain pulse arrival-time delays. The resultant Doppler delay data (with the delays due to the best-fit orbit added back in) are plotted in Figure 1.

We fit the pulse arrival time delays to circular and eccentric orbit models to obtain corrections to the provisional orbital and pulse period ephemerides. All of the models included a separate parameter for the mid-eclipse ($T_{\pi/2}$) epoch for each of the 3 observations as well as parameters for the pulse period and period derivative. We fit models in which the projected orbital radius ($a_x \sin i$) was a separate parameter for each of the 3 observations and also a model in which $a_x \sin i$ was represented by a single parameter.

In Table 3, we give the results of the fit to a model which includes separate orbital phase, pulse period, and pulse period derivative parameters for each of the three observations, but only *global* parameters for the projected orbital radius and for the orbital eccentricity. The pulse period and orbital phase zero are referenced to the solar system barycenter. We obtain a value for the eccentricity that is not statistically significant. The results presented in Table 3 and Figure 1 are based on data from the energy intervals 7-14 keV, 6-24 keV, and 2-9 keV for the 1987, 1988, and 1989 observations, respectively.

The value of 53.4875 ± 0.0009 ℓt-sec that we obtain for $a_x \sin i$ is consistent with the value of 53.46 ± 0.03 ℓt-sec found by Primini, Rappaport, and Joss (1977).

The residuals in the fits to the pulse arrival time delays are dominated by systematic effects. We arrive at this conclusion, in part, by noting that the residuals are very similar to those obtained when the analysis is performed on data from other energy ranges. Possible reasons for such systematics are (i) our lack of a complete model for the Ginga clock or (ii) effects that are actually due to some property of SMC X-1 such as the spin behavior of the neutron star, small amplitude scattering of the X-ray pulses, changes in the intrinsic pulse profile, and so forth. Most of the evidence, however, points to the Ginga clock as being the source of the few-millisecond systematic residuals.

Our determination of orbital phase zero is shown together with previous orbital phase

determinations for SMC X-1 in Figure 2. The solid curve is the best-fit to a quadratic function. The coefficient of the quadratic term of the fitting function yields $\dot{P}_{orb}/P_{orb} = (-3.34 \pm 0.02) \times 10^{-6}$ yr^{-1}. This represents highly significant evidence for orbital *decay*. This value is about a factor of two larger than the observed orbital decay rate for Cen X-3.

The orbital and other system parameters that we have determined for the SMC X-1 system are summarized in Table 4. The values for $a_x \sin i$ and $\dot{P}_{orb}/P_{orb}$ discussed above are included in the Table, as is the limit on orbital eccentricity of $e < 7 \times 10^{-5}$ (2σ confidence limit). This is presently the lowest limit on eccentricity for any of the known X-ray pulsars (true even for Her X-1?). The coefficients for the quadratic function that gives the time of the Nth eclipse in SMC X-1 are also listed in Table 4. The value of $\dot{P}_{pulse}/P_{pulse} = -5.37 \times 10^{-4}$ yr^{-1} cited in Table 4 is a fit to the long-term secular decrease in pulse period over the past 18 years. Note that the measured values of $\dot{P}_{pulse}/P_{pulse}$ determined for the three Ginga observations (Table 3) are each in reasonable accord with the long-term spin up trend. This is in sharp contrast to the situation in massive X-ray binaries where the accretion takes place via a stellar wind (e.g., 4U0900-40; references).

Values for the neutron star mass, companion star mass and radius, and orbital inclination, along with the corresponding uncertainties are also given in Table 4. These are derived from a Monte Carlo analysis which incorporates the measured system parameters, including the eclipse duration (see, e.g., Joss & Rappaport 1984; Nagase 1989, and §4.1 for more details and references).

3.2 Pulse Profiles

We used the best-fit orbital parameters to produce pulse profiles for selected time intervals from each of the three observations. Pulse profiles for 6 different energy intervals are shown in Figure 3. All of the 62 ms resolution data from the 4-day 1989 July-August observation have been used to construct these profiles. In contrast to the pulse profiles from a number of other X-ray pulsars (see, e.g., Levine et al. 1987, Nagase 1989, Levine et al. 1991) the shape of the SMC X-1 profile is nearly independent of X-ray energy over the range 2-37 keV.

Sample pulse profiles from the 1987, 1988, and 1989 observations are shown in Figure 4. While the pulse profile remains qualitatively unchanged (e.g., smoothly varying and double peaked), the detailed shape definitely changes with time time, especially the relative amplitude of the smaller of the two peaks. In particular, note that the smaller peak varied significantly over an interval of only 2 days (?) during the 1988 observation. On the other hand, it is apparent from the small residuals in our fits to the pulse arrival times (rms scatter of ~2 ms) that the phases of the two peaks in the pulse profile remain highly stable.

Finally, in Figure 5 we show a pulse profile for SMC X-1 that was constructed from 7.8

ms resolution data (during the 1989 observation). The only additional structure that is revealed which is not seen in the profiles constructed with 62 ms resolution data (Figure 3) is the small, but statistically significant, feature on the rising protion of the smaller peak at pulse phase ~0.95. Thus, the generally smooth nature of the SMC X-1 pulse profile is in contrast to the profiles of some other X-ray pulsars, especially those with longer pulse periods (e.g., 4U0900-40 and LMC X-4; McClintock et al. 1976, Levine et al. 1991).

Paragraph about the shape of the pulse profiles: (i) not sinusoidal even thought they are "smooth", (ii) the two peaks are not 180° apart (so no simple centered dipole can explain the pulse profiles).

4. Discussion

4.1 Orbital Period Changes

Observed changes in the orbital periods of massive X-ray binaries, including SMC X-1, are summarized in Table 5. Possible causes for changes in the orbital period of a binary system include mass transfer or mass loss, the gravitational influence of a third body, gravitational radiation, and tidal interactions. Kelley *et al.* (1983b) showed that conservative mass transfer was too small to explain the observed orbital period derivative of Cen X-3, and that mass loss from the binary system could explain the magnitude of the period derivative only if implausible assumptions about the rate of the mass loss and its specific angular momentum were adopted. Gravitational radiation is certainly negligible in these systems ($\dot{P}_{orb}/P_{orb} \sim -1 \times 10^{-11}$ yr^{-1}). Furthermore, there is no evidence for a nearby third body. Tidal torques, on the other hand, could plausibly produce the observed negative period derivatives in both SMC X-1 and Cen X-3; however, this requires that the companions of these systems are currently rotating more slowly than their orbits.

Previously, the orbital decay of Cen X-3 and the limits on orbital period changes in LMC X-4 have been interpreted (Kelley et al. 1983; Levine et al. 1991) in the framework of the weak friction model (Darwin 1879, Kopal 1959, Alexander 1973). We briefly review that analysis and apply it to the observed decay of the SMC X-1 orbit. In our analysis we make the simplifying assumption that the effects of mass transfer or loss can be neglected, so that the total angular momentum is constant and so that tidal interaction is the only mechanism for exchanging angular momentum between the rotation of the companion and the orbit. In this case, the total mechanical energy (orbital and rotational) decreases due to tidal friction unless the rotation frequency of the companion is synchronized to the orbit.

We define a dimensionless orbital separation $s = a/r_0$, total system angular momentum (orbital and rotational) $j = J/(I\omega_0)$, and total system energy $\varepsilon = E/(1/2\, I\omega_0^2)$, where r_0 is the orbital separation such that the orbit would have a moment of inertia equal to that of the

companion ($r_0^2 = I/\mu$), ω_0 is the corresponding Keplerian angular velocity ($\omega_0^2 = GM_T/r_0^3$), I is the moment of inertia of the companion, $\mu = M_x M_c/M_T$ is the reduced mass of the binary, M_T is the total system mass, and G is the gravitation constant (see also Darwin 1879, Counselman 1973).

The total mechanical energy is then given by the following expressions:

$$\varepsilon = (j - s^{1/2})^2 - s^{-1} \tag{1a}$$

$$\varepsilon = \Omega^2 s^{-3} - s^{-1} , \tag{1b}$$

where $\Omega = \omega_c/\omega_K$, and ω_c and ω_K are the rotation frequency of the companion and the orbital frequency, respectively. As discussed above, we have assumed that the total angular momentum remains constant as the binary system evolves tidally. Equation (1a) can be evaluated to obtain the total energy as a function of *s* for different fixed values of the total angular momentum. The results are plotted in Figure 6. The value of Ω is also important in classifying the tidal evolution. Equation (1b) is plotted in Figure 6 for different values of Ω to illustrate the correspondence of Ω with other system parameters. Each point in the (s, ε) plane (Figure 6) corresponds, in general, to two values of Ω, and, hence, to two values of *j* . We assume, however, that the rotation of the companion is prograde (i.e., that $\Omega > 0$); this implies that $s \leq j^2$. Therefore, the curves of constant *j* in Figure 6 are terminated at $s = j^2$.

In this simplified analysis, the tidal evolution may be stable or unstable (Darwin 1879, Counselman 1973, and Hut 1981). In the former case, the end point of the evolution is an equilibrium configuration characterized by corotation of the companion with the orbit. In the latter case there is no equilibrium configuration, the system cannot evolve to achieve corotation, and the system will eventually undergo catastrophic orbital decay. The dimensionless total angular momentum and orbital separation determine whether the evolution is stable. The classification of the courses of tidal evolution according to these quantities is summarized in Table 6.

We have used a Monte Carlo error propagation technique (see e.g., Joss and Rappaport 1984, Nagase 1989) to indicate regions of the (s, ε) plane in which the SMC X-1 system is likely to lie. Briefly, the ingredients for such an analysis are the projected semimajor axes of the orbits of the neutron star and companion, the X-ray eclipse angle, the moment of inertia and rotation rate of the companion star, and a parameter β which indicates the degree to which the companion star fills its Roche lobe. Since we have no direct accurate observations which yield ω_c, we simply assume Ω to be uniformly distributed over the interval 0 - 1. In the context of the tidal interaction scenario, the decay of the orbit indicates that $\Omega < 1$. The assumptions and other input to the Monte Carlo system parameter analysis are discussed in Joss and Rappaport

(1984) and Nagase (1989). The moments of inertia of massive stars (both main-sequence and evolved stars) are based on unpublished stellar evolution calculations by Podsiadlowski (1990).

The analysis of the SMC X-1 system yields a range of solutions comprising cases in which both stable and unstable orbital decay are allowed (see Fig. 6). The region of the (s, ϵ) plane occupied by SMC X-1 in which stable orbital decay is allowed is, however, quite small. This region is characterized by $1.83 < s < 2.19$ and $0.95 < \Omega < 0.97$. i.e., quite close to synchronization. All regions with $\Omega < 0.95$ correspond to systems with unstable orbital decay. We note that the region of the plane occupied by the SMC X-1 binary system is very similar to that for LMC X-4 (Levine et al. 1991), except that in the former case the region with $\Omega > 1$ has been eliminated.

In the context of the tidal evolution scenario discussed above, binaries containing neutron stars are expected to be quite eccentric just after the supernova which created the neutron star (see, e.g., Lecar, Wheeler, and McKee 1976; van den Heuvel 1983). SMC X-1, Cen X-3, and LMC X-4 all have small eccentricities, which indicates that the orbits of these systems have been circularized. Hut (1981) has shown that, for sufficiently small orbital separations, the circularization time scale is *shorter* than the synchronization time scale (cf. Lecar, Wheeler, and McKee 1976). Thus, current theory allows the possibility that systems which have circularized by tidal interactions may not yet have synchronized. The observation of a decreasing orbital period in SMC X-1 and Cen X-3 may therefore be the result of tidal torques from a companion star that is rotating less rapidly than the orbit because there has been insufficient time to achieve synchronization since the supernova which created the neutron star. The synchronization time scale becomes indefinitely long as s decreases toward $\sqrt{3}$. Indeed, if $s < \sqrt{3}$ or $j < j_{cr}$ then the system evolves unstably away from synchronization as it decays.

The above analysis, however, neglects the effects of the expansion of the companion due to its nuclear evolution, and the concomitant secular increase in mass transfer rate. These effects imply that catastrophic orbital decay is a necessary outcome, regardless of the stability of the tidal evolution predicted in the above analysis. As the companion star evolves, it will ultimately fill its Roche lobe (see §4.2). In turn, as the Roche lobe descends into the dense atmosphere of the companion, unstable mass transfer (on a thermal timescale of $\sim 10^4$ yr) will commence. Since the neutron star cannot accrete matter at rates above the Eddington limit ($\sim 10^{-8}$ $M_\odot$ yr^{-1}) most of the matter transferred through the inner Lagrange point must be ejected from the binary system. If the specific angular momentum of the ejected matter is approximately that of the neutron star, then the orbital separation will shrink rapidly. Such a situation probably leads to a phase where the neutron star spirals into the envelope of the companion possibly leading to the formation of a Thorne-Zytkow object (Thorne & Zytkow

197X; Cannon & Eggleton 1992). However, while the SMC X-1 system may be approaching this final phase of mass transfer, it is clearly not there yet.

The expansion of the companion star due to its nuclear evolution can also drive tidal decay. As the companion evolves, it expands and its moment of inertia increases. The consequent decrease in its rotation rate drives the star away from synchronous rotation. The resulting tidal torque transfers angular momentum from the orbit to the rotation of the companion, thus leading to orbital decay. Below we estimate the evolutionary expansion rate of the companion that is necessary to explain the orbital decay of SMC X-1, and we comment on the plausibility of such an expansion rate.

In the context of the weak friction model, the tidal torques on the companion star, N_c, and on the orbit, N_{orb}, may be expressed as

$$N_c = \frac{dJ_c}{dt} = \frac{d(I\omega_c)}{dt} = -\frac{(\omega_c - \omega_K)\, I}{\tau} \quad , \tag{2a}$$

$$N_{orb} = \frac{dJ_{orb}}{dt} = \frac{d(\mu a^2 \omega_K)}{dt} = \frac{(\omega_c - \omega_K)\, I}{\tau} \quad , \tag{2b}$$

where τ parameterizes the time scale of the dissipative tidal interaction. After Kepler's third law is initially used to eliminate the dependence on the orbital separation, these two equations yield the following differential equation that describes the departure from synchronous rotation as the companion star expands:

$$\frac{d(\omega_K - \omega_c)}{dt} = -\omega_c \frac{d\ln(I)}{dt} - \frac{(1 - 3I/\mu a^2)(\omega_K - \omega_c)}{\tau} \quad . \tag{3}$$

The first term on the right hand side describes the effects of the expansion of the companion, while the second term describes the effect of the transfer of angular momentum between the rotation of the companion and the orbit. This equation restates, that in the absence of expansion of the companion, and for sufficiently large separations (i.e., $s^2/3 = \mu a^2/3I > 1$), the system tends to evolve toward a synchronous state. When $s^2/3 = \mu a^2/3I$ approaches unity, the second term on the right in equation (3) decreases in magnitude. The first term may, at some point, become larger in magnitude than the second term and the expansion of the companion will then drive orbital decay. If $\mu a^2/3I$ becomes less than unity, the expansion of the companion and the instability of the tidal evolution can both drive the orbital decay.

Equation (2b) may be rewritten with the help of Kepler's third law to yield the following expression for the orbital period derivative:

$$\frac{\dot{P}_{orb}}{P_{orb}} = \frac{3I}{\mu a^2 \omega_K} \frac{(\omega_c - \omega_K)}{\tau} \quad . \tag{4}$$

The above equations are sufficient to estimate the expansion rate of the companion which is required to explain the observed orbital period derivative. To accomplish this, we assume that $\mu a^2/3I$ is sufficiently close to unity that the second term on the right side of equation (3) can be neglected in comparison with the first term. When this condition applies for a length of time Δt, we can estimate the departure from synchronism as

$$\omega_c - \omega_K \simeq \frac{d(\omega_c - \omega_K)}{dt} \Delta t = - \omega_c \Delta t \frac{d\ln(I)}{dt} \quad . \tag{5}$$

Substitution of this expression into equation (4) immediately yields

$$\frac{\dot{P}_{orb}}{P_{orb}} \simeq - \frac{\omega_c}{\omega_K} \frac{\Delta t}{\tau} \frac{d\ln(I)}{dt} \quad . \tag{6}$$

The measured value $\dot{P}_{orb}/P_{orb} \sim 3 \times 10^{-6}$ yr^{-1} may then be seen to be consistent with the following choice of parameter values: $\omega_c/\omega_K \simeq 1$, $d\ln(I)/dt \simeq 5 \times 10^{-7}$ yr^{-1} (Podsialowski 1990), and $\Delta t/\tau \sim 6$. This estimate is only valid if $\mu a^2/3I$ is sufficiently close to unity since it assumes that $|\omega_c - \omega_K|$ continues to grow for a time $\Delta t \sim 6\tau$. This will be true only if $|1 - 3I/\mu a^2| < 1/6$ or, equivalently, $1.6 < s < 1.9$. Otherwise, the second term in equation (3) grows to sufficient magnitude to limit the increase of $|\omega_c - \omega_K|$. One can also see that faster expansion rates of the companion would be able to explain the observed orbital decay rate without requiring $s^2/3 = \mu a^2/3I$ to be as close to unity. By comparison, the Monte Carlo analysis described above indicates that $1.6 < s < 2.2$ for SMC X-1.

Core hydrogen-burning stars with masses greater than ~15 $M_\odot$ have $d\ln(I)/dt \geq 5 \times 10^{-7}$ yr^{-1} (Podsialowski 1990). However, it has been noted for some time (Hutchings et al. 1979, Rappaport & Joss 1983) that the masses, radii, and luminosities of the companions in massive X-ray binaries are not quite consistent with the properties computed for isolated stars with no strong stellar winds (Iben 198x, Podsialowski 1990). Specifically, a number of the massive companion stars appear to be overluminous and have larger radii for their mass (possibly as a result of substantial mass loss via a stellar wind; see, e.g., Conti 1978, Hutchings et al. 1979, Rappaport & Joss 1983). It is difficult, therefore, to determine the present expansion rate of the companion star in SMC X-1 by comparison to the model calculations. As a consequence, we can say only that $d\ln(I)/dt \geq 5 \times 10^{-7}$ yr^{-1} is a plausible rate of evolution for the moment of inertia of the companion star, though it is hardly a secure estimate.

We conclude that expansion of the companion cannot be ruled out as the driver of orbital decay, i.e., this scenario is plausibly consistent with our knowledge of the SMC X-1 binary

system parameters and the evolutionary state of the companion star, but is otherwise unproven.

4.2 Active Lifetime of Massive X-Ray Binaries

SMC X-1 and Cen X-3 are the two massive X-ray binaries for which both the orbital decay rate and the pulsar spinup time scale are known. The orbital decay time scales for the two systems are 3×10^5 years and 5×10^5 years, respectively; the corresponding spinup time scales are 2000 and 5000 years. In each case, the ratio of these time scales is ~100. Thus, the orbital decay time scales are about 10 times shorter than the nuclear evolution time of the massive companion stars in these systems, they are about two orders of magnitude longer than the spinup time scales. It is instructive to try to reconcile these apparently disparate time scales.

To address these questions, we have constructed a very simply model to explore the evolution of the spin of the neutron stars in these systems. Consider a system consisting of a neutron star in orbit about a massive stellar companion. For a description of the earlier phases of the evolutionary history of such a system see, e.g., van den Heuvel (1983, 1986, 1990). We begin our look at the system when the neutron star is orbiting its unevolved massive companion which substantially underfills its Roche lobe. In the ~few $\times 10^6$ years until the companion evolves to fill its Roche lobe, the neutron star will have spun down from its presumably rapid rotation rate at birth to a period of the order of a second (see, e.g., Lyne and Manchester review article). Interactions of the rotating pulsar with the stellar wind of the companion will spin the pulsar down even further (references on the propeller spin-down mechanism). At some point the neutron star will begin to accrete matter from the stellar wind at a relatively slow rate (e.g., $\sim 10^{-12}\ M_\odot\ yr^{-1}$). After a relatively brief interval of such accretion the rotation rate of the neutron star will attain an equilibrium spin period given by

$$P_{eq} \simeq 0.9 \left[\frac{\dot{M}}{10^{-8} M_\odot yr^{-1}}\right]^{-3/7} \left[\frac{B}{10^{12} Gauss}\right]^{6/7} s \quad , \qquad (7)$$

(Lamb, Pethick, & Pines 1972, Rappaport & Joss 1977), which turns out to be ~18-150 s for a surface B field of 10^{12} Gauss and values of $\dot{M}$ in the range of $\sim 10^{-11}$ to $10^{-13}\ M_\odot\ yr^{-1}$.

Eventually, the companion star expands as it evolves and begins to fill a more substantial fraction of its Roche lobe. As the companion fills a large fraction of its Roche lobe, the tidal torques discussed in §4.1 become effective and the orbit will start to decay, provided that the companion is rotating more slowly than the orbit. We assume that from this point on, the orbital decay time scale is shorter than the evolutionary time scale of the companion (but see §4.1). Within a small number of orbital decay time scales, the Roche lobe begins to descend into the dense atmosphere of the companion and the final stages of the luminous X-ray phase are under way.

Following the treatment of Verbunt and Rappaport (1988), we model the orbital evolution by the following equation constructed from a simple dimensional argument:

$$\frac{dr}{dt} \simeq \frac{-R_S}{\tau_{ev}} - \frac{R_S e^{-r/H}}{\tau_{ther}} \quad , \tag{8}$$

where $r = R_L - R_S$, R_L is the mean radius of the Roche lobe, and R_S is an arbitrary reference radius near the photosphere of the companion where the gas density is sufficiently high to sustain very large mass transfer rates. The other constants in eq. (6) are τ_{ev}, the time scale over which stable evolution of the binary orbit proceeded (e.g., via tidal interaction) before the onset of the unstable mass transfer, τ_{ther} is the time scale on which the thermal-timescale mass transfer proceeds as $r \rightarrow 0$, and H is the atmospheric scale height of the companion. Briefly, the second term on the right hand side of eq. (8) is derived from the approximation that $\dot{R}_L/R_L$ is proportional to $\dot{M}/M$ (see Verbunt and Rappaport 1988) and the assumption that the mass transfer rate grows exponentially with the descent of the Roche lobe into the atmosphere. The minus sign associated with this term follows from the fact that the orbit shrinks upon conservative mass transfer from the more massive to the less massive star, i.e., the transfer will not be stable. We note that even during the *final* stages of the unstable transfer, when $\dot{M}$ greatly exceeds the Eddington limit, the matter that is necessarily ejected from the system should carry away a specific angular momentum approximately equal to that of the neutron star, in which case the sign of the proportionality in equation (8) should remain unchanged.

As shown in Verbunt and Rappaport (1988) the characteristic time scale for the growth of this runaway process is $\tau \simeq H\tau_{ev}/R_S$, i.e., the time for the tidally driven orbital decay to move the Roche lobe through an exponential scale height. For example, in the case of SMC X-1, if H is taken to be the pressure scale height at the photosphere (i.e., $\sim 0.03\ R_\odot$) then $\tau \simeq 1000$ years, a number that is comparable to the pulse period spinup time.

We can quantify the above discussion by integration of eq. (8) starting with the Roche lobe relatively far from the dense atmosphere of the companion, e.g., $r > 100$ H. As an illustrative example, we take $\tau_{ev} = 3 \times 10^5$ yr (see Table 4) and τ_{ther} to be 10^4 years (the results are insensitive to this latter choice). At each step in the integration we compute the mass transfer rate from $\dot{M}/M \simeq \exp(-r/H)/\ \tau_{ther}$. The mass transfer rate can, in turn, be used to follow the spin evolution of the neutron star. The equation that we integrated to study the spin evolution of the neutron star is

$$\frac{dP_{spin}}{dt} \simeq -1.8 \times 10^{-4}\ P_{spin}^2 \left[\frac{\dot{M}}{10^{-8} M_\odot\ yr^{-1}}\right]^{6/7} \left[\frac{B}{10^{12} Gauss}\right]^{2/7} s\ yr^{-1} \quad , \tag{9}$$

(Rappaport & Joss 1976, Ghosh & Lamb 1979). As an initial condition, we assume that when

the Roche lobe of the companion is far from its atmosphere, there is still a small steady accretion rate from the stellar wind (e.g., 10^{-12} $M_\odot$ yr^{-1}).

The results of such an integration are shown in Figure 7 for an assumed atmospheric scale height of 0.05 $R_\odot$. The evolution with time of the quantity $r = R_L - R_S$ (in units of H) is shown in Fig. 7a and the corresponding mass loss rate from the companion is given in Fig. 7b. The pulse period history along with the instantaneous value of the equilibrium pulse period are given in Figure 7c. Finally, the spinup time scale for the neutron star as a function of time is shown in Fig. 7d. Note that there is a specific time (i.e., at t = -16,000 yr) before the neutron star is engulfed in the atmosphere of the giant, when the mass transfer rate is $\dot{M} \sim 10^{-8}$ $M_\odot$ yr^{-1}, the spin period is ~0.7 s, and the spinup time scale is $P/\dot{P} \sim 3000$ years, all in agreement with the observed quantities. We find that for either substantially larger or smaller values of the atmospheric scale height, the above three parameters do not match the observed quantities simultaneously. The scale height that yields the 'best fit' is 0.05 $R_\odot$ which is a factor of ~3 larger than that calculated for the atmosphere of a massive star of the type found in SMC X-1 (see, e.g., Kurucz 1977). We note, however, that there are significant uncertainties in the equation governing the spin up of the neutron star. These include the properties of the neutron star, especially the value of its magnetic moment. We estimate that, given all of the uncertainties that we can identify, the corresponding range of allowed values of the scale height that could yield satisfactory agreement with the observed parameters at the present epoch includes $0.01\ R_\odot < H < 0.05\ R_\odot$. These values are not too far from the standard value for a nominal stellar atmosphere and do not require the kind of *ad hoc* extended exponential atmosphere of the types invoked in X-ray eclipse studies of such sources as 4U0900-40 and 4U 1538-52 (see, e.g., Lewis et al. 1992; Clark et al. 1986?).

The authors acknowledge the Ginga team for their support during the observation of SMC X-1. Two of us (AL and SR) are especially grateful for the hospitality accorded us during our stay at ISAS. We thank Ph. Podsiadlowski for providing us with some of his stellar structure and evolution calculations prior to their publication. Thanks to Jonathan Woo and John Chandler.

References

Alexander, M.E. 1973, *Ap. Sp. Sci.*, **23**, 459.

Bonnet-Bidaud, J. M., and van der Klis, M. 1981, *Astr. Ap.*, **97**, 134.

Cannon, R., and Eggleton, P. 1992, preprint

Chandler 1991 - planetary ephemeris

Clark, G.W., 1978 - position of SMC X-1

Clark, G.W., et al. 1986 - 4U1538-52 reference?

Clark, G.W., Minato, J.R., and Mi, G. 1988, *Ap. J.*, **324**, 974.

Clark, G.W., Minato, J.W., Nagase, F., Makishima, K., and Sakao, T. 1990, *Ap. J. (Letters)*, **353**, 274.

Cominsky, L.R. and Moraes, F. 1991, *Ap. J.*, **370**, 670.

Conti, P.S. 1978, A&A, **63**, 225.

Counselman, C.C. 1973, *Ap. J.*, **180**, 307.

Darwin, G.H. 1879, *Proc. Roy. Soc. London*, **29**, 168.

Darbro, W. et al. 1981, *Ap. J.*, **246**, 231.

Deeter, J.E., Boynton, P.E., Miyamoto, S., Kitamoto, S., Nagase, F., and Kawai, N. 1991, *Ap. J. (Letters)*, in press.

Deeter, J.E., and Inoue 1990

Ghosh, P., and Lamb, F.K. 1979, ApJ, **234**, 296.

Gruber, D. E. and Rothschild, R. E. 1984, *Ap. J.*, **283**, 546.

Hut, P. 1981, *Astr. Ap.*, **99**, 126.

Hutchings, J.B., Cowley, A.P., Crampton, D., van Paradijs, J., and White, N.E. 1979, ApJ, **229**, 1079.

Iben, I. Jr. 1974, ARAA, **12**, 215.; also 1983, 1985, 1986

Joss, P.C., and Rappaport, S. 1984, *Ann. Rev. Astr. Ap.*, **22**, 537.

Kelley, R. L., Jernigan, J.G., Levine, A., Petro, L.D., and Rappaport, S. 1983a, *Ap. J.*, **264**, 568.

Kelley, R. L., Rappaport, S., Clark, G.W., and Petro, L. D. 1983b, *Ap. J.*, **268**, 790.

Kopal, Z. 1959, *Close Binary Systems*, (New York: Wiley).

Kurucz, R.L. 1979, ApJS, 40, 1.

Lamb, F.K., Pethick, C.J., and Pines, D. 1972, *Ap. J.*, **184**, 271.

Lecar, M., Wheeler, J.C., and McKee, C.F. 1976, *Ap. J.*, **205**, 556.

Levine, A.M. *et al.* 1987, *Ap. J.*, **327**, 372.

Levine, A.M., Rappaport, S., Putney, A., Corbet, R., and Nagase, F. 1991, *Ap. J.*, **381**, 101.

Lewis, W., Rappaport, S., Levine, A., and Nagase, F. 1992, ApJ, in press.

Liller, W. 1973, *Ap. J. (Letters)*, **184**, L37.

Lucke, R. et al. 1976, *Ap. J. (Letters)*, **206**, L25.

Makino, F., and the ASTRO-C team, 1987, *Ap. Letters Commun.*, **25**, 223.

McClintock et al. 1976, *Ap. J. (Letters)*, **206**, L99.

Nagase, F. 1989, *Publ. Astr. Soc. Japan*, **41**,1.

Podsiadlowski, Ph. 1990, private communication.

Primini, F. Rappaport, S., and Joss, P. 1977, *Ap. J.*, **217**, 543.

Rappaport, S., and Joss, P.C. 1977, *Nature*, **266**, 683.

Rappaport, S., and Joss, P.C. 1983, in *Accretion Driven Stellar X-Ray Sources*, eds. W.H.G. Lewin and E.P.J. van den Heuvel (Cambridge, Cambridge University Press), p.

Schreier, E. *et al.* 1972, *Ap. J. (Letters)*, **178**, L71.

Seward, F. D., and Mitchell, M. 1981, *Ap. J.*, **243**, 736.

Thorne, K., and Zytkow, A. 197x

Turner, M. *et al.* 1989a, *Publ. Astr. Soc. Japan*, **41**, 345.

Turner, M.J.L. *et al.* 1989b, *23rd ESLAB Symposium on X-Ray Astronomy*, Bologna, Italy, September 1989.

van den Heuvel, E.P.J. 1983, in *Accretion Driven Stellar X-Ray Sources*, eds. W.H.G. Lewin and E.P.J. van den Heuvel (Cambridge, Cambridge University Press), p.1.

van den Heuvel, E.P.J. 1986

van den Heuvel, E.P.J. 1990

van der Klis, M., and Bonnet-Bidaud, J.M. 1981, *Astr. Ap.*, **95**, L5.

Verbunt, F., and Rappaport, S. 1988, *Ap. J.*, **332**, 193.

Webster, B., Martin, W., Feast, M., and Andrews, P. 1972, *Nature Phys. Sci.*, **240**, 183.

Table 1

Orbital Phase Measurements of SMC X-1

	N	$T_{\pi/2}$ (MJED)	Method
Uhuru	-481	40963.99 ± 0.02	eclipse ingress - egress timing
optical	-249	41866.94 ± 0.04	optical light curve
Copernicus	-144	42275.65 ± 0.04	eclipse timing
SAS-3	0	42836.1828 ± 0.0002	pulse timing
Ariel 5	42	42999.6567 ± 0.0016	pulse timing
COS-B	72	43116.4448 ± 0.0022	eclipse timing
Ginga	1055	46942.47240 ± 0.00013	pulse timing - present work
Ginga	1173	47401.744469 ± 0.000011	pulse timing - present work
Ginga	1260	47740.35910 ± 0.00004	pulse timing - present work

N is the number of orbital cycles, counted from the eclipse referenced for the SAS-3 data.

$T_{\pi/2}$ (MJED) is the orbital epoch, defined as the time when the mean longitude equals $\pi/2$. For a circular orbit this is the time of superior conjunction. Times of mid-eclipse derived from ingress and egress observations are also listed in this column.

Table 2

Ginga Pulse Height Energy Channels

Channel Number	Range of Pulse Height Energies (keV)
1	0 - 2.3
2	2.3 - 4.6
3	4.6 - 6.9
4	6.9 - 9.2
5	9.2 - 11.5
6	11.5 - 13.8
7	13.8 - 16.1
8	16.1 - 18.4
9	18.4 - 23.0
10	23.0 - 36.8

Table 3

Orbital Fits[a] for the Three SMC X-1 Observations

Parameter	Value	
$a_x \sin i$	53.4875 (9) lt-sec	
Eccentricity	< 0.00007 (2σ)	
$T_{\pi/2}$ (eclipse center, barycentric)[e]		
1987 May	MJED 46,942.47240 (13)	
1988 August	MJED 47,401.744469 (11)	
1989 August	MJED 47,740.35910 (4)	
P_{pulse} (barycentric)[b] @ Epoch		
1987 May	0.710185091(32) s	(@MJD 46941.72954)
1988 August	0.7101406731 (12) s	(@MJD 47402.52220)
1989 August	0.709809864 (43) s	(@MJD 47740.35608)
$\dot{P}_{pulse}/P_{pulse}$ (Ginga)		
1987 May	$-5.5\ (7) \times 10^{-4}$ yr^{-1}	
1988 August	$-4.54\ (2) \times 10^{-4}$ yr^{-1}	
1989 August	$-5.5\ (2) \times 10^{-4}$ yr^{-1}	

[a] All uncertainties are 1σ single-parameter confidence limits, except for the upper limit on orbital eccentricity which is 2σ. The numbers in parentheses are the uncertainties in the last digits given.

b?

c?

d?

List the definitions of MJED and MJD in the caption

Table 4

Parameters for the SMC X-1 Binary System

Parameter	Value	Uncertainty
$a_x \sin i$	53.4875 lt-s	0.0009
eccentricity	< 0.00007 (2 σ)	0.000016
$\dot{P}_{pulse}/P_{pulse}$ (long term)	-5.37×10^{-4} yr^{-1}	2×10^{-6}
a_0 (b)	MJED 42,836.18277	0.00020
a_1 (b)	3.89229073 days	5.6×10^{-7}
a_2 (b)	-6.92×10^{-8} days	0.04×10^{-8}
$\dot{P}_{orb}/P_{orb}$	-3.34×10^{-6} yr^{-1}	0.02×10^{-6}
M_C (c)	18 $M_\odot$	2.0
M_X (c)	1.1 $M_\odot$	0.2
$\theta_{eclipse}$ (d)	26.5-29°	...
inclination angle (c)	62°	4°
R_C (c)	17 $R_\odot$	1.5

What is footnote a?

b The time of the Nth eclipse can be written as: $t_N = a_0 + a_1 N + a_2 N^2$

c Based on a Monte Carlo error analysis (see, e.g., Joss and Rappaport 1984, and Nagase 1989).

d References in Joss and Rappaport 1984

Table 5

Orbital Period Changes in Massive X-Ray Binaries

Source	$\dot{P}_{orb}/P_{orb}$ (yr^{-1})	Reference
Cen X-3	$\dot{P}_{orb}/P_{orb} = -1.8 \times 10^{-6}$	Kelley et al. 1983b
SMC X-1	$\dot{P}_{orb}/P_{orb} = -3.3 \times 10^{-6}$	Present Work
LMC X-4	$\lvert\dot{P}_{orb}/P_{orb}\rvert < 2 \times 10^{-6}$	Levine et al. 1991
Her X-1	$\dot{P}_{orb}/P_{orb} \simeq -1.3 \times 10^{-8}$	Deeter et al. 1991
4U1538-52	$\lvert\dot{P}_{orb}/P_{orb}\rvert < 6 \times 10^{-6}$	Cominsky & Moraes 1991

Table 6

Constraints on Tidal Evolution

	$\Omega < 1$	$\Omega > 1$
$s < \sqrt{3}$	Unstable Decay	Stable Growth
$s > \sqrt{3}$, $j < j_{cr}$	Unstable Decay	Not Possible
$s > \sqrt{3}$, $j > j_{cr}$	Stable Decay	Stable Growth

The symbols are defined as follows: s is the dimensionless orbital separation, j is the dimensionless orbital angular momentum, and Ω is the ratio of companion rotation frequency to orbital frequency. See text for definition of the unit of length and angular momentum.

Figure Captions

Figure 1: Doppler delay data for SMC X-1 obtained from Ginga timing observations. The filled circles are the measured pulse arrival times with the effects of a constant pulse period removed. The solid curve is the best fit to a circular orbit (see text and Table 3). The residuals between the best fit and the data are shown as an "×" (note the expanded scale for the residuals).

Figure 2: Summary of mid-eclipse delay times for SMC X-1 with respect to a constant orbital period of 3.89229073 days. The SAS-3, Ariel 5, and Ginga data points are taken from Kelley *et al.* (1983b), Ariel 5 reference, and the present work, respectively. The filled circles are the measured delays of mid-eclipse as determined from pulse timing analyses; the filled triangles are from X-ray eclipse timing measurements, while the open square is from optical studies. The solid curve is the best fit of a quadratic function to the mid-eclipse delay times (see Table 4).

Figure 3: Pulse profiles of SMC X-1, in 6 energy bands, from the 1989 observations. Non-source background has been subtracted. The pulse profile is defined by 64 phase bins (~0.21-s time bins). For each pulse profile, a typical $\pm 1\sigma$ error bar due to counting statistics is shown. Data obtained during the eclipses, large flares, or times of particularly large pulse profile variability were excluded from the construction of the pulse profiles.

Figure 4: Sample pulse profiles from the 1987, 1988, and 1989 Ginga observations. Note that the relative amplitude of the smaller of the two peaks in the profile changes with time, including significant variations over an interval of only 2 days (?) during the 1988 observation.

Figure 5: Pulse profiles for SMC X-1 constructed from 7.8 ms-resolution data (during the 1989 observation). Note the small, but statistically significant, feature on the rising protion of the smaller peak at pulse phase ~0.95. The solid curves superposed on the histograms are the pulse profiles derived from the 62 ms-resolution data.

Figure 6: Binary system energy vs. orbital separation including the kinetic energy associated with the rotation of the companion star. The quantities $E_O = 1/2I\omega_o^2$ and $R_O = \sqrt{I/\mu}$ are scaling constants to cast the energy and orbital separation in dimensionless form (see text for details). The solid curves represent constant values of total angular momentum, while the dashed curves are for constant values of the parameter $\Omega = \omega_c/\omega_K$ (see text). The curve of constant total angular momentum labeled "j_{cr}" corresponds to the smallest value of j for which these curves

have a local minimum. The heavy contours represent 50% and 95% confidence limits on the measured SMC X-1 system parameters, as determined from a Monte Carlo error propagation technique (see text for details). Because of the finite bin size in which the contours are calculated, they slightly overlap the non-physical region wherein $E/E_O < -s^{-1}$.

Figure 7: Illustrative calculation of the evolutionary spin history of a neutron star in a massive binary system. (a) Difference between the Roche-lobe radius and the photospheric radius in units of the atmospheric scale height (taken to be 0.06 $R_\odot$). (b) Rate of mass loss from the donor star. (c) Pulse period (solid curve) and equilibrium spin period (dashed curve). (d) Spinup timescale.

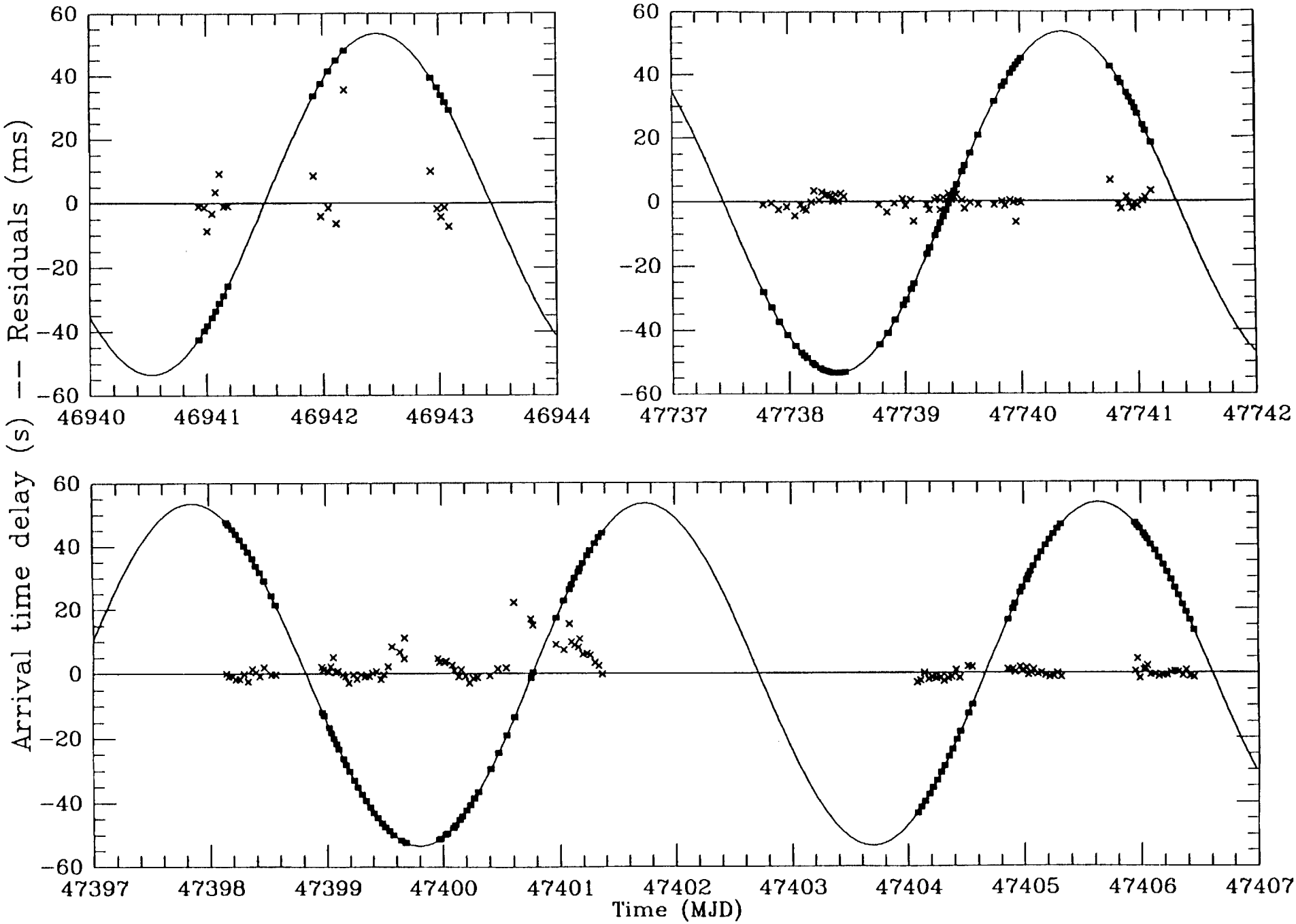
Arrival time delay (s) -- Residuals (ms)
60
40
20
0
-20
-40
-60
46940
46941
46942
46943
46944
47737
47738
47739
47740
47741
47742
47397
47398
47399
47400
47401
47402
47403
47404
47405
47406
47407
Time (MJD)

Figure 1

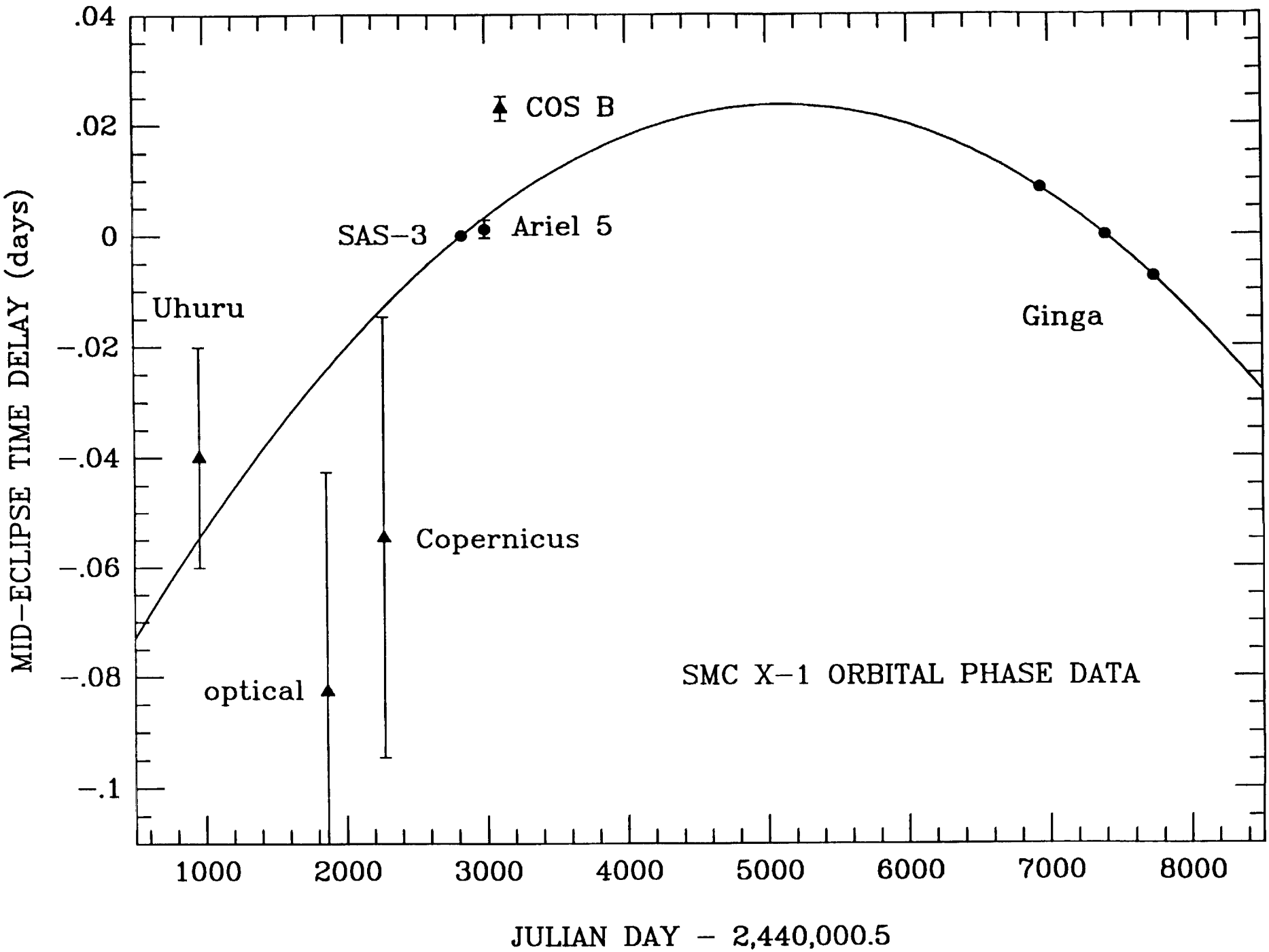
.04
.02
0
−.02
−.04
−.06
−.08
−.1
MID-ECLIPSE TIME DELAY (days)
COS B
SAS-3
Ariel 5
Uhuru
Ginga
Copernicus
optical
SMC X-1 ORBITAL PHASE DATA
1000
2000
3000
4000
5000
6000
7000
8000
JULIAN DAY − 2,440,000.5

Figure 2

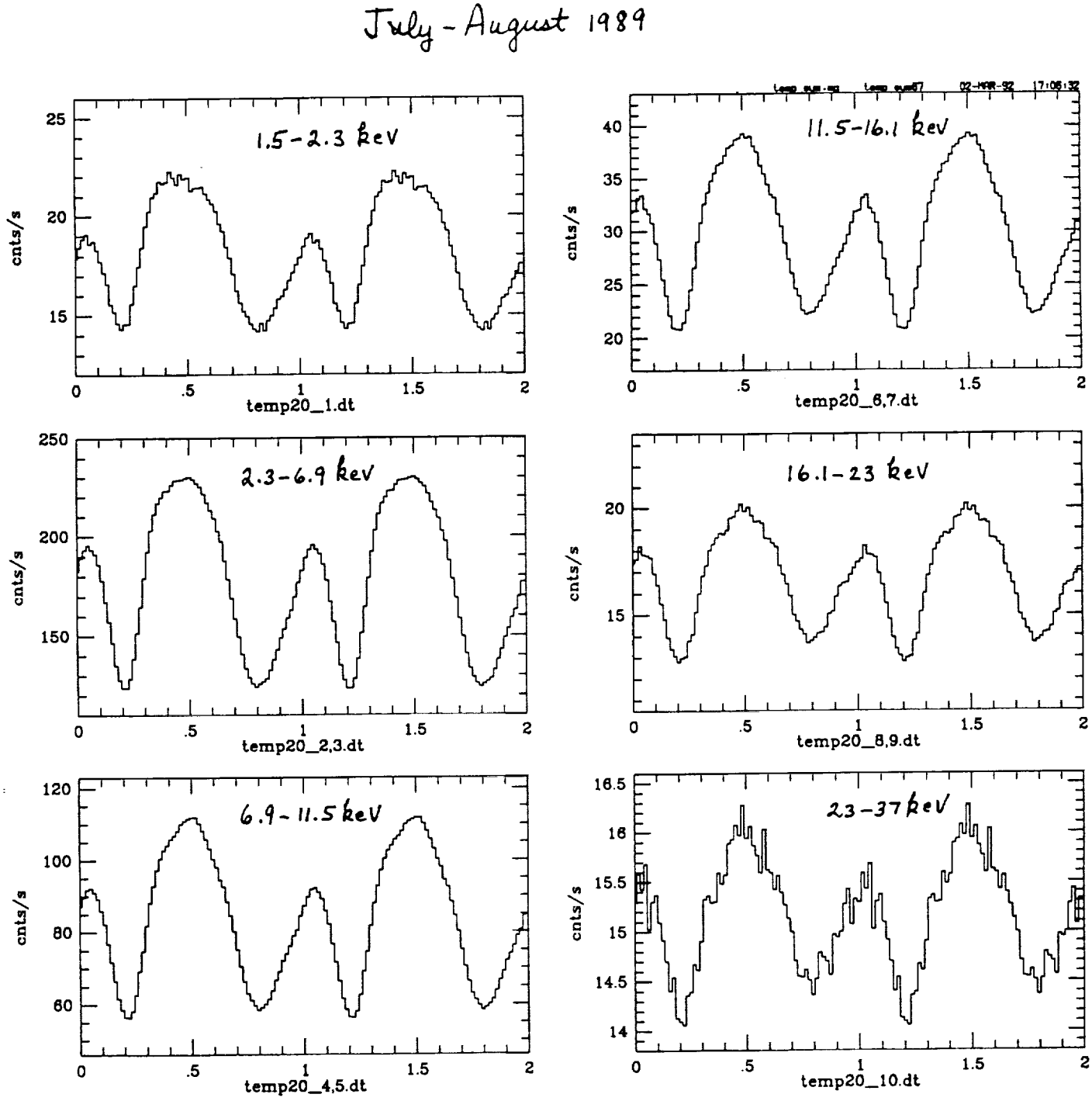
July - August 1989
1.5-2.3 keV
11.5-16.1 keV
2.3-6.9 keV
16.1-23 keV
6.9-11.5 keV
23-37 keV
cnts/s
temp20_1.dt
temp20_6,7.dt
temp20_2,3.dt
temp20_8,9.dt
temp20_4,5.dt
temp20_10.dt

Figure 3

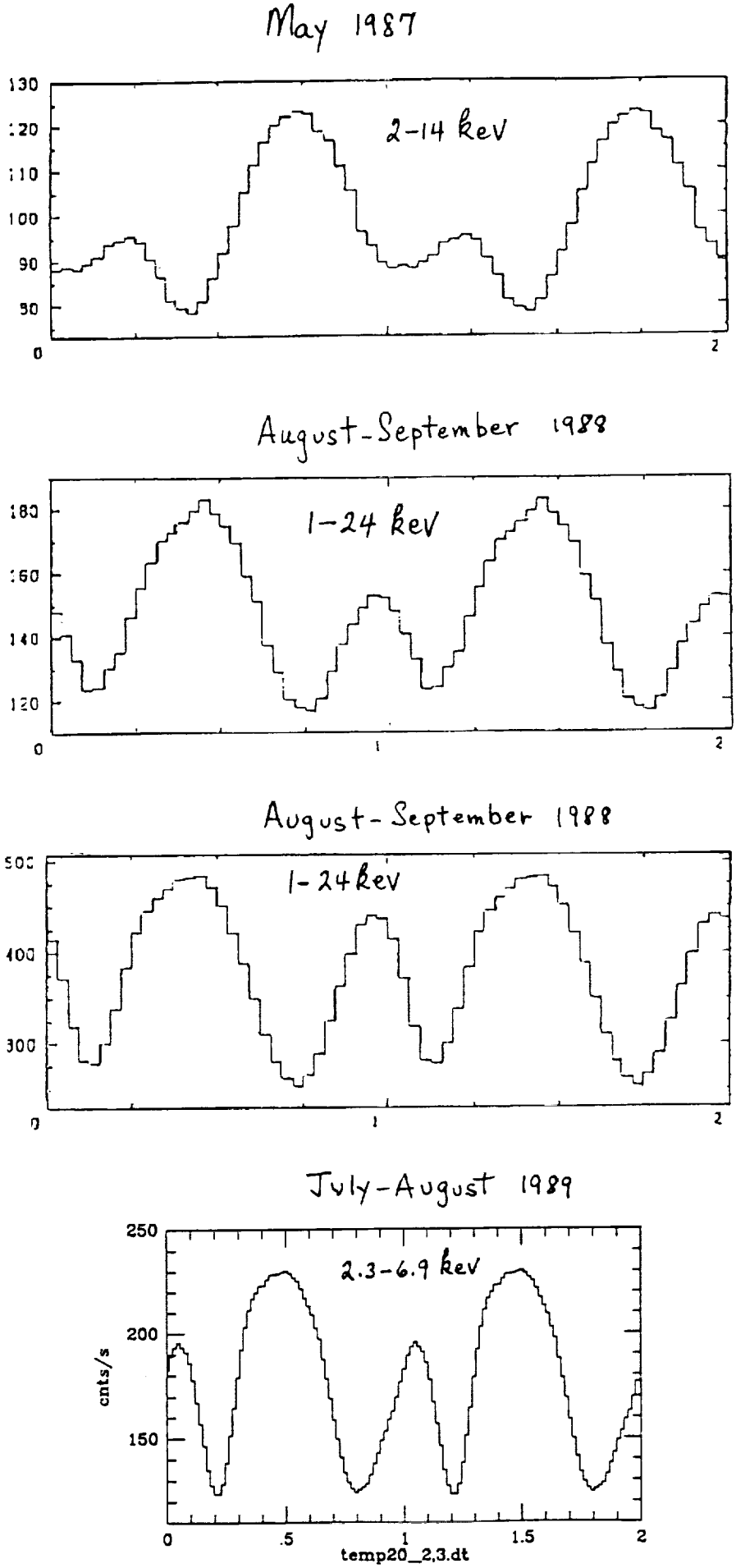
May 1987
2-14 keV
130
120
110
100
90
80
0
2
August-September 1988
1-24 keV
180
160
140
120
0
1
2
August-September 1988
1-24 keV
500
400
300
0
1
2
July-August 1989
2.3-6.9 keV
250
200
150
cnts/s
0
.5
1
1.5
2
temp20_2,3.dt

Figure 4

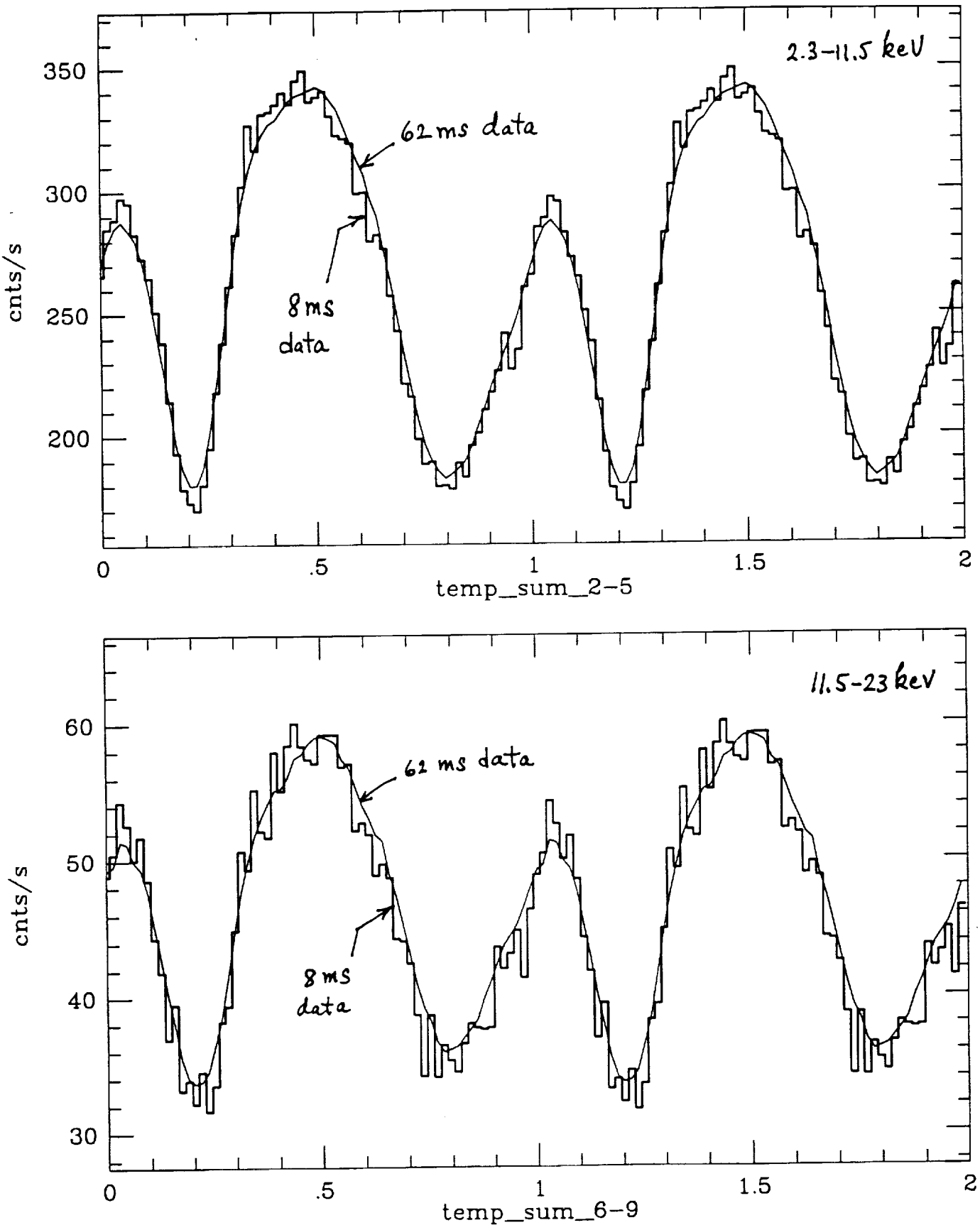
July-August 1989
2.3-11.5 keV
62 ms data
8 ms data
cnts/s
350
300
250
200
0
.5
1
1.5
2
temp_sum_2-5
11.5-23 keV
62 ms data
8 ms data
cnts/s
60
50
40
30
0
.5
1
1.5
2
temp_sum_6-9

Figure 5

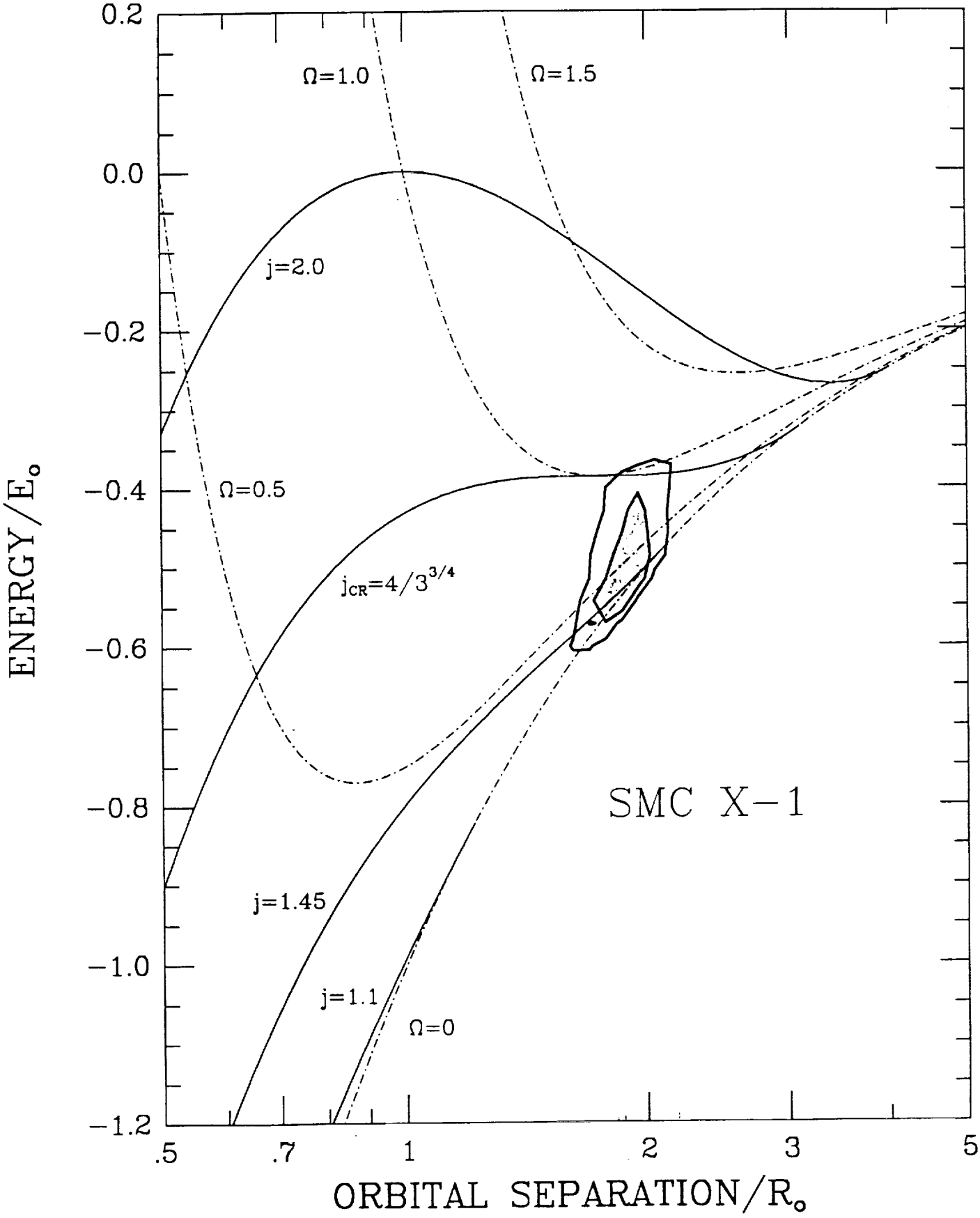
0.2
0.0
−0.2
−0.4
−0.6
−0.8
−1.0
−1.2
ENERGY/E₀
Ω=1.0
Ω=1.5
j=2.0
Ω=0.5
j_CR=4/3^3/4
SMC X−1
j=1.45
j=1.1
Ω=0
.5
.7
1
2
3
5
ORBITAL SEPARATION/R₀

Figure 6

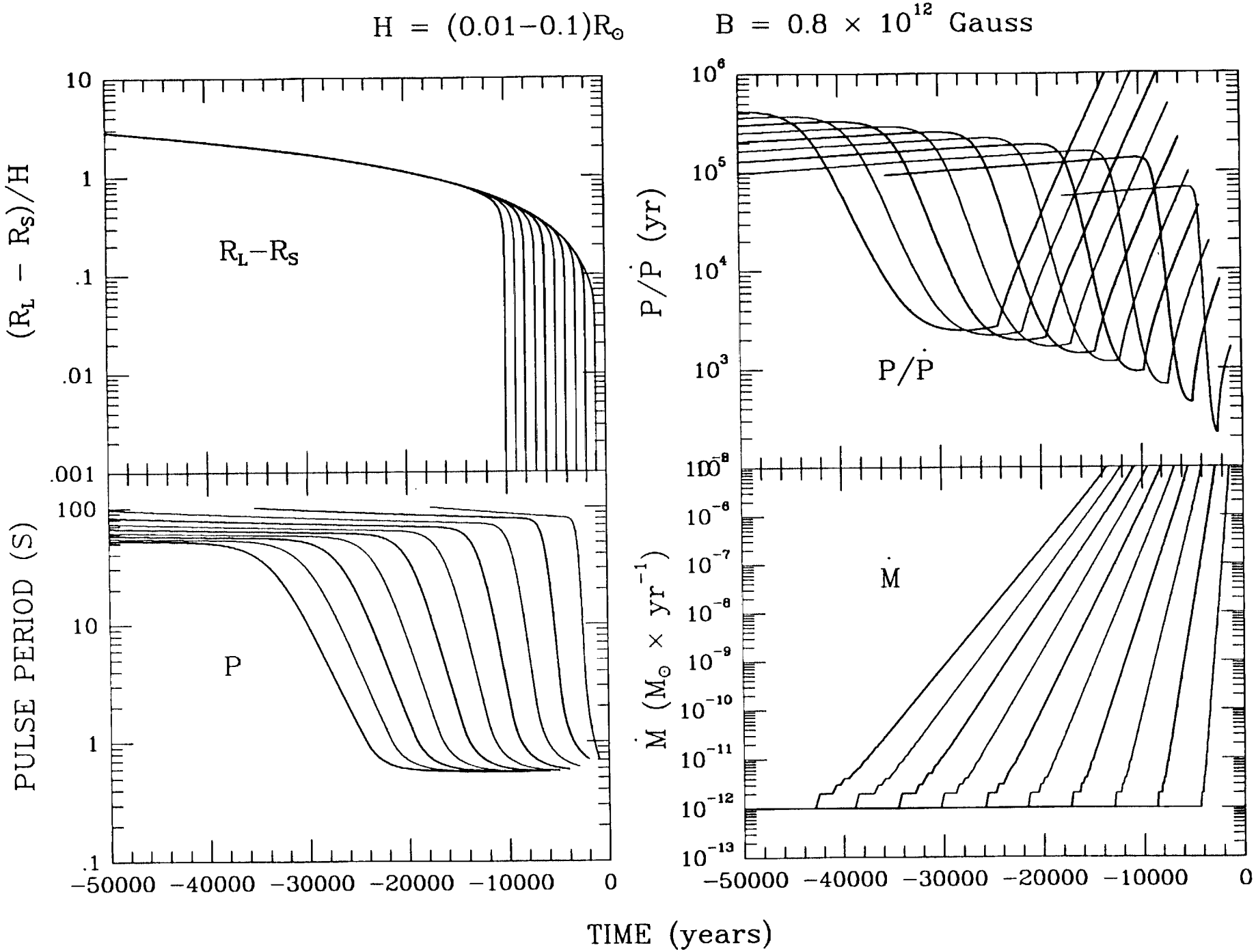
H = (0.01−0.1)R⊙
B = 0.8 × 10^12 Gauss
(R_L − R_S)/H
R_L−R_S
PULSE PERIOD (S)
P
P/Ṗ (yr)
P/Ṗ
Ṁ (M⊙ × yr^−1)
Ṁ
TIME (years)
10
1
.1
.01
.001
100
10
1
.1
10^6
10^5
10^4
10^3
10^−6
10^−7
10^−8
10^−9
10^−10
10^−11
10^−12
10^−13
−50000 −40000 −30000 −20000 −10000 0

Figure 7